Revision 1

Mg-sursassite thermo-elastic parameters and its relevance as a water carrier in subducting slabs

Milani Sula[1], Fumagalli Patrizia[1], Luca Ziberna[2], Maurice Juliette[1], Lotti Paolo[1], Comboni Davide[1,3], Pagliaro Francesco[1], Hanfland Michael[3], Bais Giorgio[4], Joseph Boby[4], Merlini Marco[1]

[1] Dipartimento di Scienze della Terra 'Ardito Desio', Università degli Studi di Milano, via Botticelli 23, 20133, Milan, Italy

[2] Dipartimento di Matematica e Geoscienze, Università degli Studi di Trieste, via Weiss 8, 34128, Trieste, Italy

[3] ESRF-European Synchrotron Radiation Facility, 71 Avenue des Martyrs, CS40220, Grenoble Cedex, 38043, France

[4] Elettra-Sincrotrone Trieste S.C.p. A., Strada Statale 14 km 163.5, Basovizza, Trieste, 34149, Italy

Abstract

We report the synthesis, at 7 GPa and 923 K, and the thermoelastic characterization, up to 16 GPa and 850 K, of single crystal of Mg-sursassite, $Mg_5Al_5Si_6O_{21}(OH)_7$. In-situ high-pressure and high-temperature single crystal diffraction allowed the study of structural variation at non-ambient conditions and the determination of bulk elastic properties. The refined parameters of a second order Birch-Murnagham Equation of State (BM-II EoS) are V_0= 446.02(1) Å^3 and K_{T0} = 135.6(7) GPa. The thermal expansion coefficients of a Berman-type EoS are α_0=3.14 (5) x 10^{-5} K^{-1}, α_1=2.50(16) x 10^{-8} K^{-2} and V_0=445.94(3). For comparison, the *P-V* Equation of State is determined for a natural sursassite sample, ideally $Mn_4Al_6Si_6O_{22}(OH)_6$. The refined parameters of BM-II EoS (V_0 = 470.2(3) Å^3, K_{T0}=128(4) GPa) indicate that composition has a minimal effect on elastic properties. The similarity of density and bulk properties of Mg-sursassite if compared to olivine and other anhydrous mantle minerals suggests that this phase could be overseen by geophysical methods.

Keywords: Mg-sursassite, hydrous minerals, structure, thermo-elastic parameters.

1. Introduction

The deep-water cycle plays a fundamental role in the evolution of Earth and has a strong influence on life creation and sustainability. High-pressure and high-temperature experimental petrology shows that the number of possible hydrous phases that can carry water into the Earth's mantle via subduction is quite broad. The determination of the stability field of these hydrous phases and of the mechanism of sequestration and release of water accomplished through their occurrence are paramount to unravel the evolution of our 'water' planet. Mg-sursassite is one of these hydrates. This phase has been first synthesized in the simple $MgO-Al_2O_3-SiO_2-H_2O$ (MASH) system with either a Ca-free or MgMg-Al pumpellyite structure (Schreyer et al. 1986; Fockenberg 1998) or in a disordered pumpelleyite structure with local sursassite-type geometry (Artioli et al. 1999). Its crystal structure has been further constrained using Rietveld method and transmission electron microscopy to an isostructural arrangement as Mn-sursassite $Mn_4Al_2Al_4Si_6O_{22}(OH)_6$. In this, Mn to Mg substitution takes place together with Al replacement by Mg + H, thus giving a nominal chemical formula of $Mg_5Al_5Si_6O_{21}(OH)_7$ and hence has been referred as Mg-sursassite (Gottschalk et al. 2000).

Mg-sursassite is a sorosilicate mineral, that forms after the breakdown of layered minerals like chlorite and retains water in its structure. It belongs to the group of 'Dense Hydrous Magnesium-Aluminum Silicates' (DHMAS). As the majority of DHMAS and Dense Hydrous Magnesium Silicates' (DHMS), Mg-sursassite is characterised by a modulated-layered structure. The main characteristic of DHMS/DHMAS is that they are stable and they can bear a large amount of 'water' (e.g. phase E can hold up to 18wt% of H_2O) even under extreme conditions, P = 13-18 GPa and T = 1573 K (Purevjav et al. 2020 and references therein). Indeed, they represent the major group of minerals which have a large hydrogen storage capacity over a wide pressure and temperature range (Purevjav et al. 2020), contributing therefore to the global water budget, which is one of the key topics for understanding the nature and evolution of the Earth's interior, since water can affect mantle rheology, melting temperature and electrical conductivity (e.g. Smyth 2006).

It has been already demonstrated that Mg-sursassite ($Mg_5Al_5Si_6O_{21}(OH)_7$), containing about 7 wt% H_2O, can be a possible high-pressure carrier of significant volumes of H_2O in a range of bulk compositions from pelitic (Domanik and Holloway 1996) to mafic/ultramafic compositions (Fockenberg 1998; Artioli et al. 1999, Bromiley and Pawley 2002). Indeed, its stability field was originally defined in the interval 6–7 GPa and < 973 K, allowing water transfer in the subducting slab from chlorite minerals to the high pressure dense hydrous magnesium silicate phase A. For instance, a chlorite-bearing peridotite containing 2.8 wt% H_2O could provide the transfer of 0.98 wt% H_2O via the reaction chlorite+enstatite=Mg-sursassite+forsterite+fluid (Luth 2003). Recently, a Si-rich Mg-sursassite with octahedrally coordinated Si (Bindi et al. 2020), has brought more attention to this phase, because it was synthesized at more extreme conditions of 24 GPa and 1673 K, broadening the stability field of this phase and casting new light on the fate of this phase in cold subducting slabs.

Recently, other new hydrous high-pressure phases in the MASH system were identified at mantle conditions (Fumagalli et al. 2014; Cai et al. 2015; Gemmi et al. 2016) as candidate water carriers in deep H_2O cycle. It is unlikely to recover natural samples of these candidate minerals, therefore the determination of their physical and thermodynamic properties is the main means of understanding the possibility of indirectly identifying them through geophysical methods.

We have been successful in synthesising large Mg-sursassite crystals which permitted us to carry out structural characterizations with in-situ diffractometric techniques. In this paper we report the thermo-elastic and structural behaviour of Mg-sursassite at high-pressure or high-temperature, obtained by in-situ single crystal X-ray diffraction techniques at synchrotron radiation facilities, in relation with its mineral composition. The results will constitute a valuable experimental dataset, fundamental for any further study.

2. Experimental methods

Synthetic large single crystals (up to 200x100x100 μm^3) of Mg-sursassite were obtained at high pressure and high temperature using a multi-anvil module at the Department of Earth Sciences, University of Milan (DES-UM). A gel of stoichiometric composition, modelled in the MASH system, was used as a starting material prepared following the procedure adopted by Hamilton and Henderson (1968). Platinum capsules (3.5 mm length and 2 mm diameter) were welded after being loaded with the gel and saturated with water, which was added with a micro-syringe. Cr-doped MgO octahedra of 25 mm of edge length were used as pressure cell in 32 mm edge length tungsten carbide cubes. Graphite heaters were used, and temperatures were measured by a Pt-PtRh thermocouple (S-type). Temperature is accurate to ± 20 K, with no pressure correction for e.f.m. of thermocouple. Pressure uncertainties were assumed ± 3% according to the accuracy of calibrant reactions (Fumagalli and Poli 2005). Samples of Mg-sursassite were synthesized at 7 GPa and 923 K (ramp rate at about 35 K/min) with a run duration of 72 hours. The multi-anvil experiment was performed with a Cr-doped MgO octahedron of 25 mm edge length combined with tungsten carbide cubes of 15 mm truncation-edge lengths. For the experiment a graphite heater was employed. All the minerals were characterized via preliminary single crystal X-ray diffraction measurements. Mineral composition of selected Mg-sursassite crystals was determined via electron microprobe analysis (EMPA) at the DES-UM using a Jeol 8200 electron microprobe operating at 15 nA and 15 kV, with standard of pyrope for both Si and Mg.

A synthetic single crystal of Mg-sursassite (~60 x 50 x 15 μm^3) was picked from the experimental charge and glued on a glass fiber, which was attached on a metallic pin. The single-crystal x-ray diffraction measurement was carried out at the DES-UM at room temperature using a four circles κ-geometry Rigaku XtaLAB Synergy diffractometer equipped with a PhotonJet (Mo) X-ray Source, operating at 50 kV and 1 mA, with a monochromatized Mo$K\alpha$ radiation, and with a Hybrid Pixel Array detector at 150 mm from the sample position. The measurement strategy was programmed with a combination of scans in ω with

0.5° step and with an exposure time of 3.5 s at each scan step for different 2θ, κ and ϕ positions. Data reductions, including Lorenz-polarization and absorption correction based on the implemented semi-empirical ABSPACK routine, were performed using the software CrysAlisPro (Rigaku Oxford Diffraction 2019).

For comparison, a natural sample of sursassite single crystal $(Mn^{2+}_{1.61}Ca_{0.39})_{\Sigma 2}(Mn_{0.25}Al_{2.33}Mg_{0.33}Fe^{3+}_{0.01})_{\Sigma 2.92}Si_{3.08}O_{10.49\text{-}10.74}(OH)_{3.26\text{-}3.51})$ from La Falotta (Switzerland), kindly provided by the Museum of Mineralogy at the DES-UM, was also studied. We assume the chemical composition reported in Nagashima et al. (2009) for this natural sample. This natural crystal was selected for the absence of pumpelleyite domains in these samples (Nagashima et al. 2009) and for the possibility to pick up a single crystal of suitable size for high-pressure studies.

In-situ high-pressure (H*P*) single crystal X-ray diffraction measurements have been carried out at the beamline ID15b of the European Synchrotron Radiation Facility (ESRF, Grenoble), loading a synthetic single crystal of Mg-sursassite in a Diamon-Anvil Cell (DAC). The standard H*P* single crystal diffraction setup was used (Merlini and Hanfland 2013). Wavelength was 0.41130 Å. The pressure transmitting medium used in this experiment was neon, which transmits pressure hydrostatically up to the maximum pressure reached in this study of about ca. 16 GPa (Klotz et al. 2009). The H*P* experiment on the natural sursassite was instead performed at the Italian Synchrotron (Elettra, Trieste) H*P* beamline Xpress (Lotti et al. 2020) up to ca. 6 GPa. Wavelength was 0.49450 Å and the detector used was a MAR345 imaging plate. For this experiment the pressure transmitting medium was a 4:1 methanol:ethanol mixture, which transmits pressure hydrostatically up to the pressure reached in this measurement (Klotz et al. 2009). In both the experiments ruby fluorescence was used as a pressure standard (Mao et al. 1986; Chervin et al. 2001).

In-situ high-temperature (H*T*) single crystal X-ray diffraction experiment was carried out at the XRD1 beamline at the Italian Synchrotron (Elettra, Trieste). Wavelength was 0.7000 Å and the detector used was Pilatus 2M. A synthetic single crystal of Mg-sursassite, together with a single crystal of quartz used as standard, were loaded in a quartz-glass capillary and during the measurement crystals were kept steady with quartz-glass fibres. The data were collected every 30 K in a temperature range from 318 to 823 K. Temperature was maintained with a hot gas blower.

3. Results and discussion

3.1 Crystal-chemical formula of Mg-sursassite

Ten data points were measured on a sample of Mg-sursassite by EMPA and the composition of the single point-analyses is shown in Table 1. The average empirical formula calculated from the ten analyses and based on 16 cations a.p.f.u. is $Mg_{4.96(10)}Al_{4.93(8)}Si_{6.11(8)}O_{21.15}(OH)_{6.85}$. It is noticeable a slight excess of Si against nominal formula with six Si atoms a.p.f.u., which may occupy partially the smaller [6]-coordinated sites. The OH content is derived from charge balance.

3.2 Crystal structure of Mg-sursassite

The single crystal X-ray diffraction measurements confirm that the structure is monoclinic. The refined unit cell from laboratory data is a = 8.5375 (16) Å, b = 5.7097 (11) Å; c = 9.6477 (17) Å, β = 108.340 (17)° and V = 446.40 (15) Å^3. The structural refinement was handled via Jana2006 software (Petricek et al. 2014) starting from the atomic coordinates of a published crystal structure (Nagashima et al. 2009) in the space group $P2_1/m$. The Mg-sursassite is a sorosilicate characterized by layers of 6-coordinated sites (Fig.1a). As reported in Nagashima et al. (2009) the structure is characterized by two bigger 6-coordinated sites where the bivalent cation is located (Mg1 and Mg2), while the trivalent cation, Al, occupies the two smaller 6-coordinates sites (Al2, Al3). A further octahedral site has an intermediate volume if compared to MgO6 and AlO6 octahedra, and this site has likely a mixed Mg-Al occupancy (Fig. 1a). As it can be seen from the Fourier differences of the electron density (Fig. 1b) there are some maxima close to O11, O7 and O6, where the H cations might be located, in agreement with literature data (Nagashima et al. 2009). The principal statistical parameters of the structure refinement are listed in Table 2. Atomic coordinates and site occupancies of structure refinements are given in Table S1. Anisotropic displacement parameters and relevant bond distances are reported in Table S2, S3. The crystallographic information file is available as Supplementary Materials.

3.3 Compressibility behavior of Mg- and natural sursassite

The evolution of the unit-cell volume of Mg-sursassite at different pressures is reported in Table 3. The volume decreases smoothly with increasing pressure, as shown in Fig. 2, up to the maximum hydrostatic conditions reached in this study of ca. 16 GPa. No phase transition or change of the deformation mechanisms occur within the *P*-range investigated. The *P–V* data were fitted using a second-order Birch–Murnaghan EoS (BM2-EoS; Birch 1947), since the Eulerian finite strain (f_e) vs. normalized stress (F_e) plot (F_e–f_e plot, Fig. S1a) of the data can be fitted by a horizontal straight line (Angel 2000). The BM2-EoS coefficients were refined simultaneously, data were weighted by their uncertainties in *P* and *V*, using the program EoSFit-7c (Angel et al. 2014) giving: V_0= 446.1(1) Å^3, K_{T0} = 135.6(7) GPa and K'=4 fixed (ΔPmax=-0.35 GPa, χ^2w=1.92). The calculated ΔP_{max} and χ^2w values indicate that the EoS provide a good fit to the data.

Crystal structure refinements at variable pressures indicate that compression of the octahedral sites is function of their size, with the two Mg-sites more compressible than Al and (Al, Mg) sites. Silicon tetrahedral sites are much more incompressible (Fig. S2).

The unit-cell parameters of the natural sursassite decrease smoothly with increasing pressure to the maximum conditions reached in the experiment as shown in Fig. 3 and reported in Table S4. The experimental data were suitable only for lattice parameter determination. No phase transition or change of the deformation mechanisms occur within the *P*-range investigated (Fig.3). *P-V* data were fitted with a BM2-EoS (Birch 1947), because the F_e–f_e plot (Fig. S1b) of the data can be fitted with a horizontal line (Angel 2000). As for the Mg-sursassite case, the BM2-EoS coefficients were refined simultaneously and the data were weighted by their uncertainties in P and V using the program EoSFit-7c (Angel et al. 2014). The so obtained coefficients are: V_0 = 470.2(3) Å^3, K_{T0}=128(4) GPa and K'=4 fixed.

Note that the values of K_{T0} for natural and synthetic sursassite are the same within error, demonstrating no significant influence of composition on the value of the bulk modulus. Up to date only one study determined the bulk modulus of the Mg-sursassite (Grevel et al. 2001). This study has been carried out on a powder sample up to 7.52 GPa and the P-V data are fitted with a BM2-EoS (Birch 1947) giving the following parameters: V_0 = 446.49 Å3, K_{T0}=116(1.3) and K'=4. The pressure transmitting medium in these experiments is vaseline, which is known not to transmit the pressure hydrostatically above 3 GPa (Tateiwa and Haga 2009), therefore the difference in the results could be due to a different experimental protocol.

3.4 Thermal expansion behavior of Mg-sursassite

The temperature (T) – volume (V) data collected during the experiment at ambient pressure are reported in Fig. 4 and Table 4. As it can be observed from Fig. 4, V increases continuously without any phase transition, any change of the deformation mechanisms or any evidence of an irreversible change in the crystal during the experiment up to the maximum T reached in the study. The V-T data were fitted using EosFit 7c (Angel et al. 2014) using a Berman-type EoS (Berman 1988). The thermal expansion coefficient obtained are: α_0=3.14 (5) x 10^{-5} K^{-1}, α_1=2.50(16) x 10^{-8} K^{-2} and V_0=445.94(3) (χ^2_w=1.34). Data points 2, 3 and 16 were omitted in the fitting, due to an oscillation of the temperature during the data collection.

For sake of comparison between data presented in this study and those published by Grevel et al. (2001) data were re-fitted with a thermal pressure model (Holland and Powell 2011) using the program EoSFit-

7c (Angel et al. 2014). The Einstein temperature (θ_E) used to fit the data is 575.19 K. This value was estimated following Holland and Powell (2011), with entropy (S) taken from Grevel et al. (2001). The parameters obtained from the fitting are listed in Table 5. The main difference is visible in the value of the bulk-modulus of about 15 GPa (Table 5).

Single crystal structure refinements at variable temperatures reveal an inverse relationship of structural parameters (Hazen and Finger 1982) if compared to high-pressure data, with polyhedral volume expansion greater in Mg-octahedral sites than in Al-sites and a much lower expansion in tetrahedral sites (Fig. S3).

4. Implications and conclusions

Synthesis of Mg-sursassite at 7 GPa and 923 K resulted in large prismatic single crystals up to 200x100x100 μm^3. Single crystal X-ray diffraction analysis indicates a pure sursassite structural model, without macroscopically detectable defects or intergrowths can well describe the data. It is worth noting that there is a slight excess of tetrahedrally coordinated Si, suggesting that the excess atoms are in the octahedral sites. The presence of octahedrally coordinated Si in Mg-sursassite has already been reported by Bindi et al. (2020), but their sample was synthesised at higher pressure and temperature (24 GPa and 1673 K) with respect to our sample (7 GPa and 923 K). The presence of octahedrally coordinated Si in the sample synthesised in this study is in agreement with the so called majoritic substitution that occurs at pressures greater than ~ 5 GPa and this represents the coupled substitution of Si and Mg (and Fe) onto the octahedrally coordinated site that occurs in garnets within mantle assemblages as a result of the breakdown of both orthopyroxene and clinopyroxene (Ringwood 1967).

Our H*P* diffraction study provides the bulk modulus of Mg-sursassite, K_{T0} to be 135.6(7) GPa. The obtained bulk modulus shows that its behaviour is stiffer with respect to DHMS such as phase A or phase 10Å (Crichton and Ross 2000; Comodi et al. 2006), or if compared also to new high-pressure hydrous phases in MASH system such as 11.5 Å, 23 Å and Hyso phase (Table 6). The compressibility of Mg-sursassite is comparable to forsterite and superhydrous phase B. Another important point worth of notice is that the values of the bulk moduli of synthetic Mg-sursassite and natural sursassite do not change significantly as function of composition implying that the effect of the composition variation on the elastic properties is almost irrelevant.

The thermoelastic values of Mg-sursassite extracted from this study might bear important implications about the detectability of this phase in the mantle by geophysical methods since these values are like the elastic parameters of nominally anhydrous mantle silicates. If we try to model the variation of the density (g/cm^3) of the Mg-sursassite with respect to a Mg_2SiO_4 (forsterite, fo) to 13 GPa (base of the upper mantle) we can observe that the difference is ca. of 1.15% (Fig. 5). If we assume that Mg-sursassite is a stable phase in the subducting slab down to the base of the upper mantle, this density difference might be too low to allow its detectability by geophysical methods from minerals like olivine (Fig. 5). In Fig. 5 we can also observe how the values of the thermoelastic parameters determined in our study with respect to already published data influence the estimation of its density at upper mantle conditions.

Further studies are needed to constrain the properties and stability of Mg-sursassite and its possible solid solutions. This is because i) Mg-sursassite is a breakdown product of chlorite, which is considered the major water carrier at mantle depth in a cold slab subduction system (e.g. Fumagalli et al. 2014; Gemmi et al. 2016; Bromiley and Pawley 2002), ii) it can be stable up to pressures of the mantle transition zone (Bindi et al. 2020) and therefore may not be any longer only a link as a water carrier between the breakdown of the chlorite and the formation of phase A (Fumagalli et al., 2014; Bromiley and Pawley, 2002), and iii) its elastic properties, comparable to those of nominally anhydrous mantle silicates, suggest that this phase can be overseen by geophysical methods.

Acknowledgment

European Synchrotron Radiation Facility is acknowledged for provision of beamtime at ID15B beamline. Elettra synchrotron facility is acknowledged for provision of beamtime at XPRESS and XRD1 beamline. The research leading to this result has been supported by the project CALIPSOplus under Grant Agreement 730872 from the EU Framework Programme for Research and Innovation HORIZON 2020. We acknowledge Andrea Risplendente for microprobe analysis and the "Museo delle Collezioni Mineralogiche" of the Earth Science department (Univ. Milano) for provision of natural sursassite sample. SM, PF, JM, PL, FP and MM acknowledge the support of the Italian Ministry of Education (MIUR) through the project "Dipartimenti di Eccellenza 2018–2022". We are thankful to two anonymous reviewers for detailed and constructive comments, which helped to improve the manuscript substantially.

References

Angel, R.J. (2000) Equations of state. In R.M. Hazen and R.T. Downs, Eds., High-Temperature and High-Pressure Crystal Chemistry, 41, p 35-59. Reviews in Mineralogy and Geochemistry, Mineralogical Society of America, Chantilly, Virginia.

Angel, R.J., and Jackson, J.M. (2002) Elasticity and equation of state of orthoenstatite, $MgSiO_3$. American Mineralogist, 87, 558-561.

Angel, R.J., Gonzales-Platas, J., and Alvaro, M. (2014) EoSFit7c and a Fortran module (library) for equation of state calculations. Zeitfrisch fur Kristallographie, 229, 405-419.

Angel, R.J., Alvaro, M., and Nestola, F. (2018) 40 years of mineral elasticity: a critical review and a new parameterisation of equations of state for mantle olivines and diamond inclusions. Physics and Chemistry of Minerals, 45, 95-113.

Artioli, G., Fumagalli, P., and Poli, S. (1999). The crystal structure of $Mg_8(Mg_2Al_2)Al_8Si_{12}(O,OH)_{56}$ pumpellyite and its relevance in ultramafic systems at high pressure. American Mineralogist, 84, 1906-1914.

Berman, R.G. (1988) Internally-consistent thermodynamic data for minerals in the system Na_2O-K_2O-CaO-MgO-FeO-Fe_2O_3-Al_2O_3-SiO_2-TiO_2-H_2O-CO_2. Journal of Petrology, 29, 445-522.

Bindi, L., Welch, M.D., Bendeliani, A.A., and Bobrov, A.V. (2020) Si-rich Mg-sursassite $Mg_4Al_5Si_7O_{23}(OH)_5$ with octahedrally coordinated Si: A new ultrahigh-pressure hydrous phase. American Mineralogist, 105, 1432–1435.

Birch, F. (1947) Finite elastic strain of cubic crystals. Physical Review, 71, 809–824.

Bromiley, G.D., and Pawley, A.R. (2002) The high-pressure stability of Mg-sursassite in a model hydrous peridotite: a possible mechanism for the deep subduction of significant volumes of H_2O. Contribution to Mineralogy and Petrology, 142, 714-723.

Cai, N., Kikegawa, T., and Inoue, T. (2018) Compressibility of the 23 Å phase under high pressure and high temperature. Physic of the Earth and Planetary Interiors, 283, 1-6.

Cai, N., Inoue, T., Fujino, K., Ohfuji, H., and Yurimoto, H. (2015) A possible new Al-bearing hydrous Mg-silicate (23 angstrom phase) in the deep upper mantle. American Mineralogist, 100, 2330-2335.

Chantel, J., Manthilake, G.M., Frost, D.J., Beyer, C., Boffa Ballaran, T., Jing, Z., and Wang, Y. (2016) Elastic wave velocities in polycrystalline Mg3Al2Si3O12-pyrope garnet to 24 GPa and 1300 K. American Mineralogist, 101, 991-997.

Chervin, J.C., Canny, B., and Mancinelli, M. (2001) Ruby-spheres as pressure gauge for optically transparent high pressure cells. High Pressure Research, 21, 305-314.

Comodi, P., Fumagalli, P., Montagnoli, M., and Zanazzi, P.F. (2004) A single-crystal study on the pressure behavior of phlogopite and petrological implications. American Mineralogist, 89, 647-653.

Comodi, P., Cera, F., Dubrovinsky, L., and Nazzareni, S. (2006) The high-pressure behaviour of the 10 Å phase: a spectroscopic and diffractometric study up to 42 GPa. Earth and Planetary Science Letters, 246, 444-457.

Crichton, W.A., Ross, N.L., and Gasparik, T. (1999) Equations of state of magnesium silicates anhydrous B and superhydrous B. Physics and Chemistry of Minerals, 26, 570-575.

Crichton, W.A., and Ross, N.L. (2000) Equation of state of phase E. Mineralogical Magazine, 64, 561-567.

Crichton, W.A., and Ross, N.L. (2002) Equation of state of dense hydrous magnesium silicate phase A, $Mg_7Si_2O_8(OH)_6$. American Mineralogist, 87, 333-338.

Domanik, K.J., and Holloway, J.R. (1996) The stability and composition of phengitic muscovite and associated phases from 5.5 to 11 GPa: Implications for deeply subducted sediments. Geochimica et Cosmochimica Acta, 60, 4133-4150.

Fockenberg, T. (1998) An experimental study of the pressure-temperature stability of MgMgAl-pumpelleyite in the system MgO-Al_2O_3-SiO_2-H_2O. American Mineralogist, 83, 220-227.

Fumagalli, P., and Poli, S. (2005) Experimentally determined phase relations in hydrous peridotites to 6.5 GPa and their consequences on the dynamics of subduction zones. Journal of Petrology, 46, 555-578.

Fumagalli, P., Poli, S., Fischer, J., Merlini, M., and Gemmi, M. (2014) The high-pressure stability of chlorite and other hydrates in subduction mélanges: experiments in the system Cr_2O_3-MgO-Al_2O_3-SiO_2-H_2O. Contributions to Mineralogy and Petrology, 167, 979.

Gatta, G.D., Merlini, M., Valdrè, G., Liermann, H.-P., Nénert, G., Rothkirch, A., Kahlenberg, V., and Pavese, A. (2013) On the crystal structure and compressional behavior of talc: a mineral of interest in petrology and material science. Physics and Chemistry of Minerals, 40, 145-156.

Gemmi, M., Merlini, M., Palatinus, L., Fumagalli, P., and Hanfland, M. (2016) Electron diffraction determination of 11.5 Å and HySo structures: Candidate water carriers to the Upper Mantle. American Mineralogist, 101, 2645-2654.

Gottschalk, M., Fockenberg, T., Grevel, K.-D., Wunder, B., Wirth, R., Schreyer, W., and Maresch, W.V. (2000) Crystal structure of the high-pressure phase $Mg_4(MgAl)Al_4[Si_6O_{21}/(OH)_7]$: an analogue of sursassite. European Journal of Mineralogy, 12, 93-945.

Grevel, K.-D., Navrotsky, A., Kahl, W.A., Fasshauer, D.W., and Majzlan, J. (2001) Thermodynamic data of the high-pressure phase $Mg_5Al_5Si_6O_{21}(OH)_7$ (Mg-sursassite). Physics and Chemistry of Minerals, 28, 475-487.

Hamilton, D.L., and Henderson, C.M.B. (1968) The preparation of silicate composition by gelling method. Mineralogical Megazine, 36, 832-838.

Hazen, R., and Finger, L. (1982) Comparative crystal chemistry, 231 p. Wiley, New York.

Holland, T.J.B., and Powell, R. (2011) An improved and extended internally consistent thermodynamic dataset for phases of petrological interest, involving a new equation of state for solids. Journal of Metamorphic Geology, 29,333 - 383.

Klotz, S., Chervin, J-C, Munsch, P., and Le Marchand, G. (2009) Hydrostatic limits of 11 pressure transmitting media. Journal of Physics D: Applied Physics, 42, 075413.

Lotti, P., Milani, S., Merlini, M., Joseph, B., Alabarse, F., and Lausi, A. (2020) Single-crystal diffraction at the high-pressure Indo-Italian beamline Xpress at Elettra, Trieste. Journal of Synchrotron Radiation, 27, 222-229.

Luth, R.W. (2003) Mantle Volatiles – Distribution and Consequences. In H.D. Holland and K.K. Turekian, Eds., The Mantle and Core, 2, p. 319-361. Treatise on Geochemistry. Elsevier Ltd.

Mao, H.K., Xu, J., and Bell, P.M. (1986) Calibration of the ruby pressure gauge to 800 kbar under quasi-hydrostatic conditions. Journal of Geophysical Research, 91, 4673-4676.

Merlini, M., and Hanfland, M. (2013) Single crystal diffraction at megabar conditions by synchrotron radiation. High-Pressure Research, 33, 511–522.

Momma, K., and Izumi, F. (2011) *VESTA 3* for three-dimensional visualization of crystal, volumetric and morphology data. Journal of Applied Crystallography, 44, 1272-1276.

Nagashima, M., Akasaka, M., Minakawa, T., Libowitzky, E., and Armbruster, T. (2009) Sursassite: hydrogen bonding, cation order, and pumpellyite intergrowth. American Mineralogist, 94, 1440–1449.

Nestola, F., Boffa-Ballaran, T., Balic-Zunic, T., Princivalle, F., and Dal Negro, A. (2007) Comparative compressibility and structure behavior of spinel $MgAl_2O_4$ at high pressure: the independency on degree of cation order. American Mineralogist, 92, 1838-1843.

Nestola, F., Angel, R.J., Zhao, J., Garrido, C.J., López Sánchez-Viscaíno, V., Capitani, G., and Mellini, M. (2010) Antigorite equation of state and anomalous softening at 6 GPa: an in situ single-crystal X-ray diffraction study. Contributions to Mineralogy and Petrology, 160, 33-43.

Pawley, A.R., Clark, S.M., and Chinnery, N.J. (2002) Equation of state measurements of chlorite, pyrophyllite, and talc. American Mineralogist, 87, 1172-1182.

Petricek, V., Dusek, M., and Palatinus, L. (2014) Crystallographic Computing System JANA2006: General features. Zietschrift fur Kristallographie, 229, 345-352.

Purevjav, N., Okuchi, T., and Hoffman, C. (2020) Strong hydrogen bonding in a dense hydrous magnesium silicate discovered by neutron Laue diffraction. IUCrJ, 7, 370-374.

Rigaku Oxford Diffraction, CrysAlisPro Software system, version 1.171.40.67a (2019), Rigaku Corporation, Wroclaw, Poland.

Ringwood, A.E. (1967) Pyroxene–garnet transition in the Earth's mantle. Earth and Planetary Science Letters, 2, 255–263.

Schreyer, W., Maresch, W.V., Medenbach, O., and Baller, T. (1986) Calcium free pumpellyite, a new synthetic hydrous Mg-Al silicate found at high-pressures. Nature, 321, 510-511.

Smyth, J.R. (2006) Hydrogen in High Pressure Silicate and Oxide Mineral Structures. In H. Keppler and J.R. Smyth, Eds., Water in Nominally Anhydrous Minerals, 62, p 85-110. Reviews in Mineralogy and Geochemistry, Mineralogical Society of America, Chantilly, Virginia.

Tateiwa, N., and Haga, Y. (2009) Evaluations of pressure-transmitting media for cryogenic experiments with diamond anvil cell. Review of Scientific Instruments, 80, 123901.

van Keken, P.E., Kiefer, B., and Peacock, S.M. (2002) High-resolution models of subduction zones: Implications for mineral dehydration reactions and the transport of water into the deep mantle. Geochemistry, Geophysics, Geosystems, 3, 1056.

Welch, M.D., Gatta, G.D., and Rotiroti, N. (2011) The high-pressure behavior of orthorhombic amphiboles. American Mineralogist, 96, 623-630.

Figure captions

Figure 1 (**a**) crystal structure of the Mg-sursassite projected parallel to [0 1 0], (**b**) as in (**a**) but superimposed are the Fourier-difference maxima close to O6, O7 and O11, where the H atoms are located. All the representations of the structure are realized using the program VESTA (Momma and Izumi 2011).

Figure 2 Evolution of the unit-cell volume with pressure of the Mg-sursassite. The solid line represents the 2nd order BM-EoS fit.

Figure 3 Evolution of the unit-cell volume with pressure of the natural sursassite. The solid line represents the 2nd order BM-EoS fit.

Figure 4 Evolution of the unit-cell volume with temperature of the Mg-sursassite. Data were fitted with a Berman type EoS (solid line).

Figure 5 Evolution of the density of Mg-sursassite along a *P*-*T* path representative of the top (solid line) and bottom (dashed line) of a cold subducting slab (based on the isoviscous model of van Keken et al. 2002). Thermodynamic data for forsterite (fo) are from Holland and Powell (2011). Mg-sursassite is indicated as Mg-surs. Density has been calculated using the equation of state for solids from Holland and Powell (2011).

Table 1. Major element composition (in wt%) of Mg-sursassite synthesised in this work. Each column represents the analysis of one crystal in the experimental charge.

SiO_2	41.28	40.91	43.20	40.84	41.70	41.53	41.95	41.18	41.70	41.36
Al_2O_3	28.12	28.2	28.93	29.04	28.11	28.13	27.96	28.97	28.11	28.59
MgO	21.48	21.16	23.00	22.88	22.92	22.98	23.10	22.67	23.13	22.80
tot	90.88	90.27	95.12	92.77	92.73	92.64	93.02	92.82	92.95	92.74
(apfu)										
Si	6.21	6.19	6.19	5.99	6.12	6.10	6.14	6.04	6.10	6.07
Al	4.98	5.03	4.89	5.02	4.86	4.87	4.82	5.01	4.85	4.94
Mg	4.81	4.78	4.92	5.00	5.01	5.03	5.04	4.96	5.05	4.99
average										
Si	6.11(8)									
Al	4.93(8)									
Mg	4.96(10)									

380

Table 2. Details pertaining to the data collections and structure refinements of the Mg-sursassite studied in this work.

a (Å)	8.5375(16)
b (Å)	5.7097(11)
c (Å)	9.6477(17)
β (Å)	108.340(17)
V (Å^3)	446.40(15)
Space group	$P2_1/m$
λ (Å)	0.71073
θ_{max} (°)	27.18
No. measured reflections	5808
No. unique reflections	1053
No. refined parameters	124
No. restraints	0
R_{int}	0.0382
R_1 (F)	0.0306
wR_2 (F^2)	0.0412
GooF	1.83
Residuals (e$^-$/Å^3)	-0.44/+0.56

381

Table 3. Lattice parameters of Mg-sursassite at different pressures, collected using neon as *P*-transmitting medium (*P*-uncertainty: ±0.05 GPa).

P (GPa)	*a* (Å)	*b* (Å)	*c* (Å)	*β* (°)	*V* ($Å^3$)
0.001	8.508(4)	5.7158(4)	9.6498(9)	108.13(2)	445.98(17)
0.08	8.4910(2)	5.6849(3)	9.6012(4)	108.183(10)	445.88(1)
0.21	8.5275(7)	5.7023(1)	9.6398(2)	108.298(5)	445.05(15)
0.53	8.5221(9)	5.6977(1)	9.6305(2)	108.259(6)	444.07(15)
1.17	8.5060(2)	5.6921(3)	9.6156(4)	108.212(10)	442.26(13)
1.82	8.4910(2)	5.6849(3)	9.6012(4)	108.183(10)	440.34(12)
2.54	8.4744(10)	5.6778(2)	9.5866(2)	108.134(7)	438.32(13)
3.34	8.4538(7)	5.6663(1)	9.5632(2)	108.076(5)	435.48(15)
3.94	8.4409(4)	5.6600(1)	9.5504(1)	108.056(3)	433.81(10)
4.13	8.4373(4)	5.6583(1)	9.5470(1)	108.046(3)	433.35(10)
4.47	8.4306(5)	5.6551(1)	9.5398(2)	108.022(3)	432.50(12)
5.32	8.4132(6)	5.6461(1)	9.5217(2)	107.982(3)	420.20(12)
5.92	8.3997(6)	5.6395(1)	9.5079(2)	107.947(4)	428.48(12)
6.60	8.3840(8)	5.6305(1)	9.4907(2)	107.915(5)	426.30(13)
7.44	8.3670(2)	5.6255(2)	9.4778(4)	107.861(14)	424.61(12)
8.02	8.3540(2)	5.6175(2)	9.4624(4)	107.833(13)	422.73(19)
8.81	8.3430(2)	5.6118(2)	9.4509(4)	107.806(12)	421.26(12)
9.60	8.3260(2)	5.6031(2)	9.4334(4)	107.765(14)	419.09(11)
10.40	8.3100(2)	5.5940(2)	9.4163(4)	107.736(14)	416.94(11)
11.05	8.3000(2)	5.5871(2)	9.4027(4)	107.708(15)	415.38(12)
11.90	8.2860(2)	5.5801(2)	9.3891(4)	107.684(12)	413.6(12)
12.41	8.2780(3)	5.5752(3)	9.3788(5)	107.655(18)	412.48(12)
12.78	8.2760(2)	5.5734(2)	9.3758(4)	107.654(14)	412.09(11)
13.47	8.2561(9)	5.5612(1)	9.3551(2)	107.642(5)	409.33(15)
14.87	8.2379(9)	5.5515(1)	9.3364(2)	107.605(5)	406.98(14)
15.88	8.2246(13)	5.5439(1)	9.3224(2)	107.574(7)	405.23(19)

Table 4. Lattice parameters of Mg-sursassite at different temperatures, collected in a quartz vial (*T*-uncertainty: ± 1 K).

T (K)	*a* (Å)	*b* (Å)	*c* (Å)	*β* (°)	*V* (Å^3)
317	8.5392(4)	5.7078(2)	9.6498(4)	108.324(4)	446.483(3)
342	8.5417(2)	5.7094(9)	9.6533(2)	108.333(2)	446.878(13)
372	8.5455(2)	5.7091(2)	9.6530(2)	108.352(2)	446.987(16)
401	8.5491(2)	5.7113(1)	9.6560(2)	108.365(2)	447.449(14)
431	8.5529(2)	5.7126(3)	9.6597(2)	108.376(2)	447.898(13)
460	8.5571(2)	5.7137(2)	9.6632(2)	108.382(2)	448.354(18)
490	8.5604(2)	5.7157(9)	9.6669(2)	108.394(2)	448.822(13)
519	8.5643(2)	5.7177(1)	9.6704(2)	108.403(2)	449.322(14)
549	8.5683(2)	5.7191(1)	9.6744(2)	108.412(2)	449.802(14)
578	8.5727(2)	5.7205(2)	9.6791(2)	108.418(2)	450.350(19)
608	8.5765(2)	5.7224(2)	9.6825(2)	108.429(3)	450.829(2)
638	8.5801(2)	5.7245(1)	9.6864(2)	108.439(2)	451.340(14)
667	8.5842(2)	5.7262(1)	9.6906(2)	108.447(2)	451.863(14)
697	8.5879(2)	5.7280(2)	9.6953(2)	108.459(2)	452.385(16)
726	8.5901(2)	5.7290(2)	9.6983(2)	108.464(2)	452.712(15)
756	8.5961(2)	5.7321(2)	9.7038(2)	108.469(2)	453.511(15)
785	8.6004(2)	5.7341(2)	9.7094(2)	108.473(2)	454.151(15)
815	8.6034(2)	5.7353(2)	9.7142(2)	108.467(2)	454.646(17)

Table 5. Thermo-elastic parameters of Mg-sursassite fitted by a Thermal pressure model (Holland and Powell 2011).

V_0 (Å^3)	K_{T0} (GPa)	K'	α_0 (x 10^{-5} K^{-1})	Reference
446.00(5)	135.5(9)	4	2.95(4)	This work
446.25(15)	120.03	4	2.74(8)	Grevel et al. (2001)

Table 6. Comparison of bulk moduli of Mg-sursassite and other hydrous and anhydrous phases in MASH system.

Mineral	K_{T0} (GPa)	K'	V_0 (Å^3)	EoS	Reference
Mantle olivine	126.3(2)	4.54(5)	291.5	BM III	Angel et al. (2018)
orthoenstatite	105.7(1.9)	8.4(6)	832.5(2)	BM III	Angel and Jackson (2002)
antophyllite	65.8(1.6)	10.5(1.1)	1766.07(3)	BM III	Welch et al. (2011)
pyrope	170.8(1.5)	4.43(8)	-	BM III	Chantel et al. (2016)
spinel	192(1)	5.4(3)	528.39(2)	BM III	Nestola et al. (2007)
talc	56(3)	5.4(7)	454.7(10)	BM III	Gatta et al. (2013)
phlogopite	54(2)	7(1)	497.1(1)	BM III	Comodi et al. (2004)
antigorite	62.9(4)	6.1(2)	2914.07(23)	BM III	Nestola et al. (2010)
chlorite	89.5(3)	4	699.2	BM II	Pawley et al. (2002)
Mg-sursassite	135.6(7)	4	446.01(10)	BM II	This study
11.5 Å phase	108.3(2)	4	1066.53(2)	BM II	Gemmi et al. (2016)
23 Å phase	111(1)	4	538.0(3)	BM II	Cai et al. (2018)
HySo	120.6(6)	4	676.8(3)	BM II	Gemmi et al. (2016)
10 Å phase	39(3)	12.5(8)	492.9(3)	BM III	Comodi et al. (2006)
phase A	97.5(4)	5.97(14)	512.56(3)	BM III	Crichton and Ross (2002)
Shy-B	142.6(8)	5.8(2)	624.71(3)	BM III	Crichton et al. (1999)
phase E	92.9(7)	7.3(2)	105.627(7)	BM III	Crichton and Ross (2000)
Anhy-B	151.5(9)	5.5(3)	838.86(4)	BM III	Crichton et al. (1999)

386

Figure 1

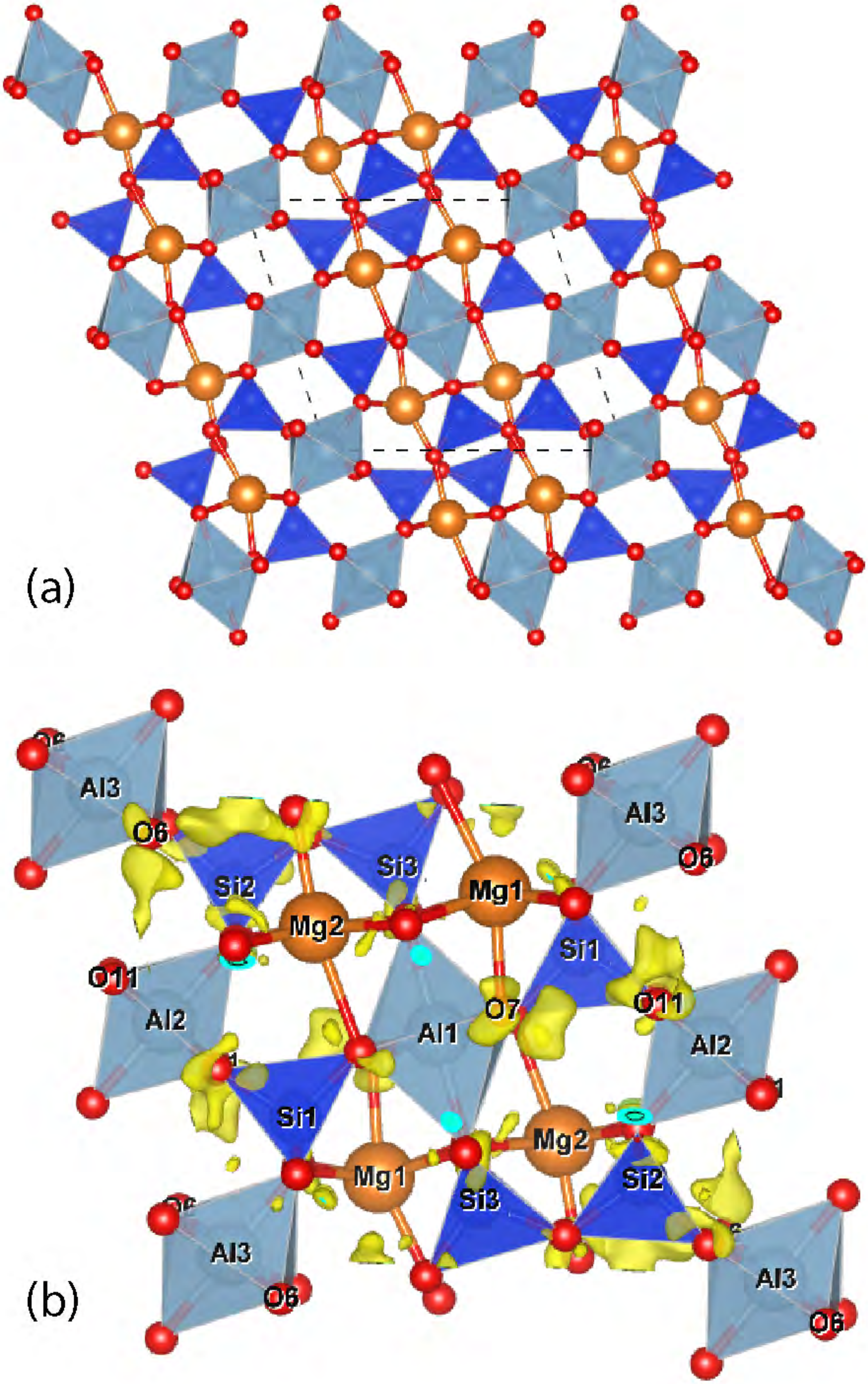
(a)
(b)
Al3
O6
Si2
Si3
Mg1
Mg2
O11
Al2
Al1
O7
Si1
Al2
Mg2
Mg1
Si3
Si2
Al3
O6
Al3
O6
Al3
O6
O11

Figure 2

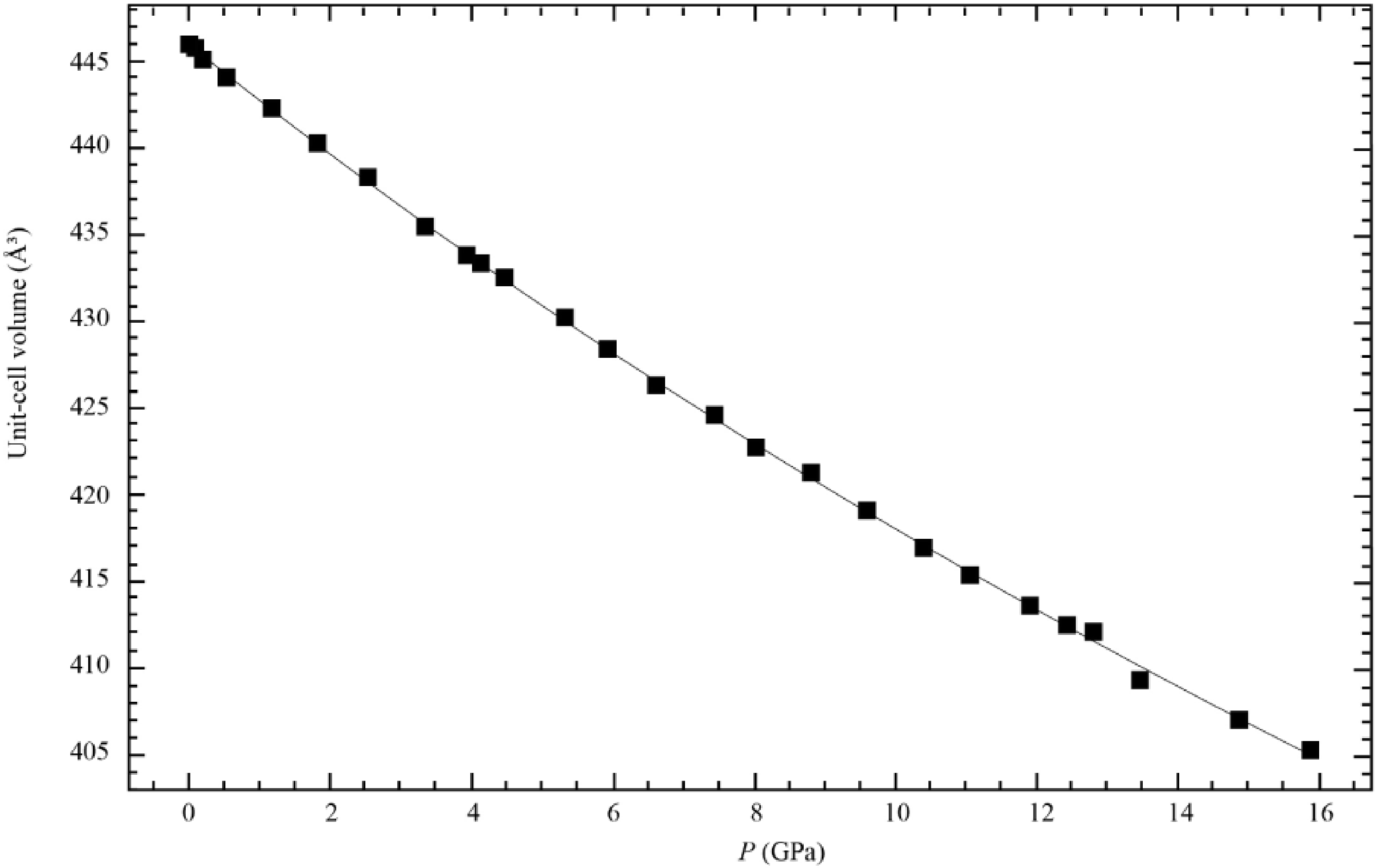
Unit-cell volume (Å³)
445
440
435
430
425
420
415
410
405
0
2
4
6
8
10
12
14
16
P (GPa)

Figure 3

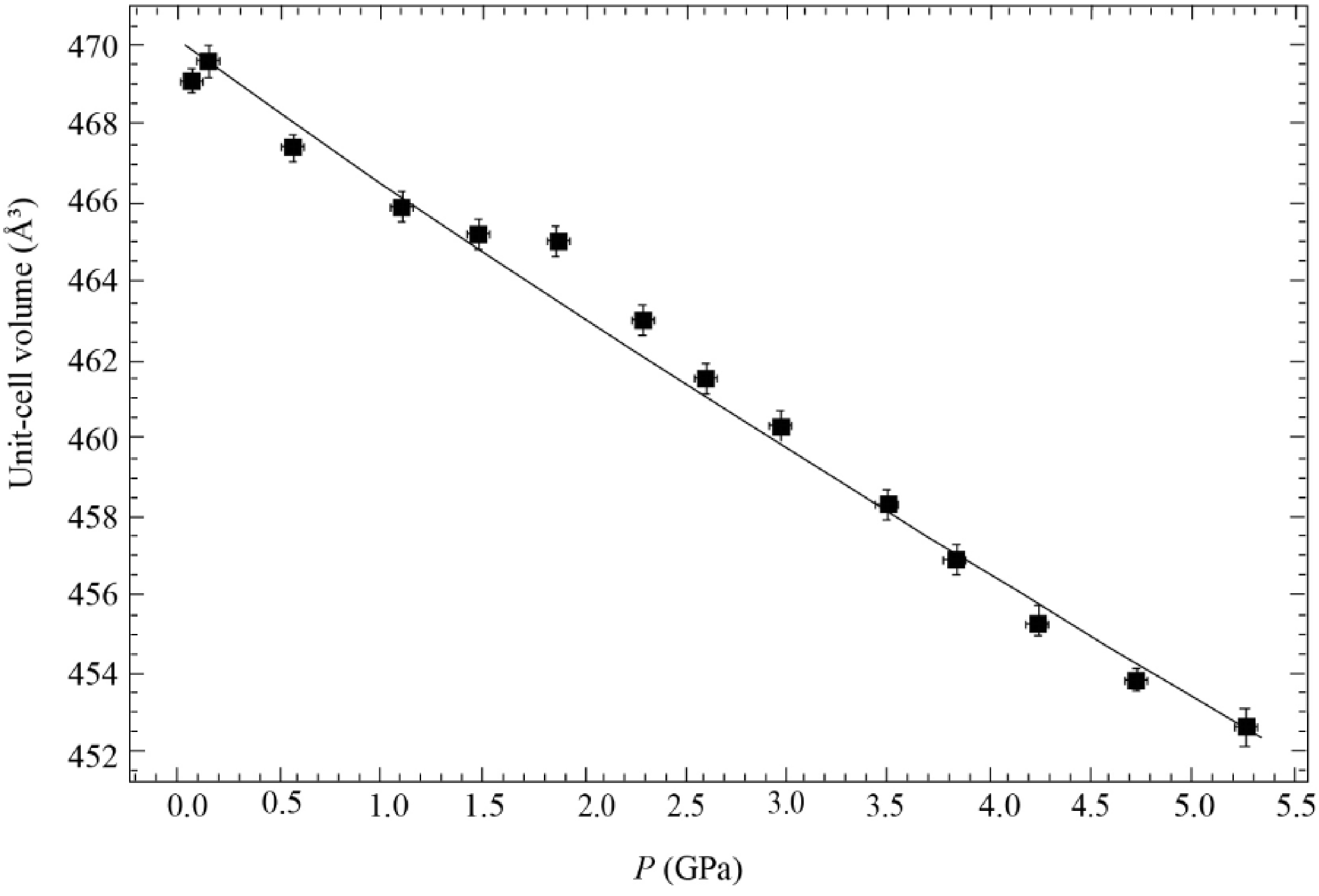
Unit-cell volume (Å³)
470
468
466
464
462
460
458
456
454
452
0.0
0.5
1.0
1.5
2.0
2.5
3.0
3.5
4.0
4.5
5.0
5.5
P (GPa)

Figure 4

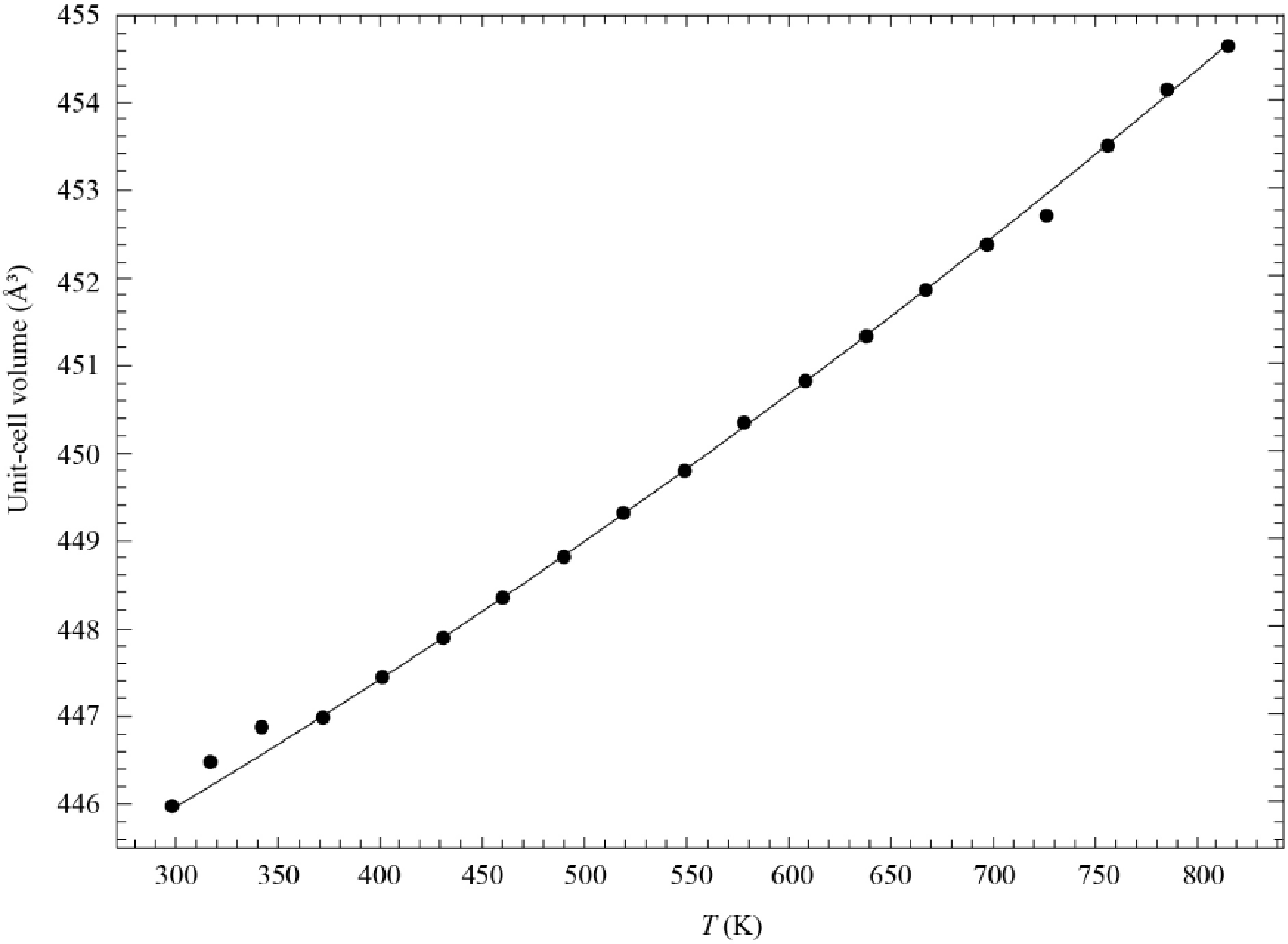
455
454
453
452
451
450
449
448
447
446
Unit-cell volume (Å³)
300
350
400
450
500
550
600
650
700
750
800
T (K)

Figure 5

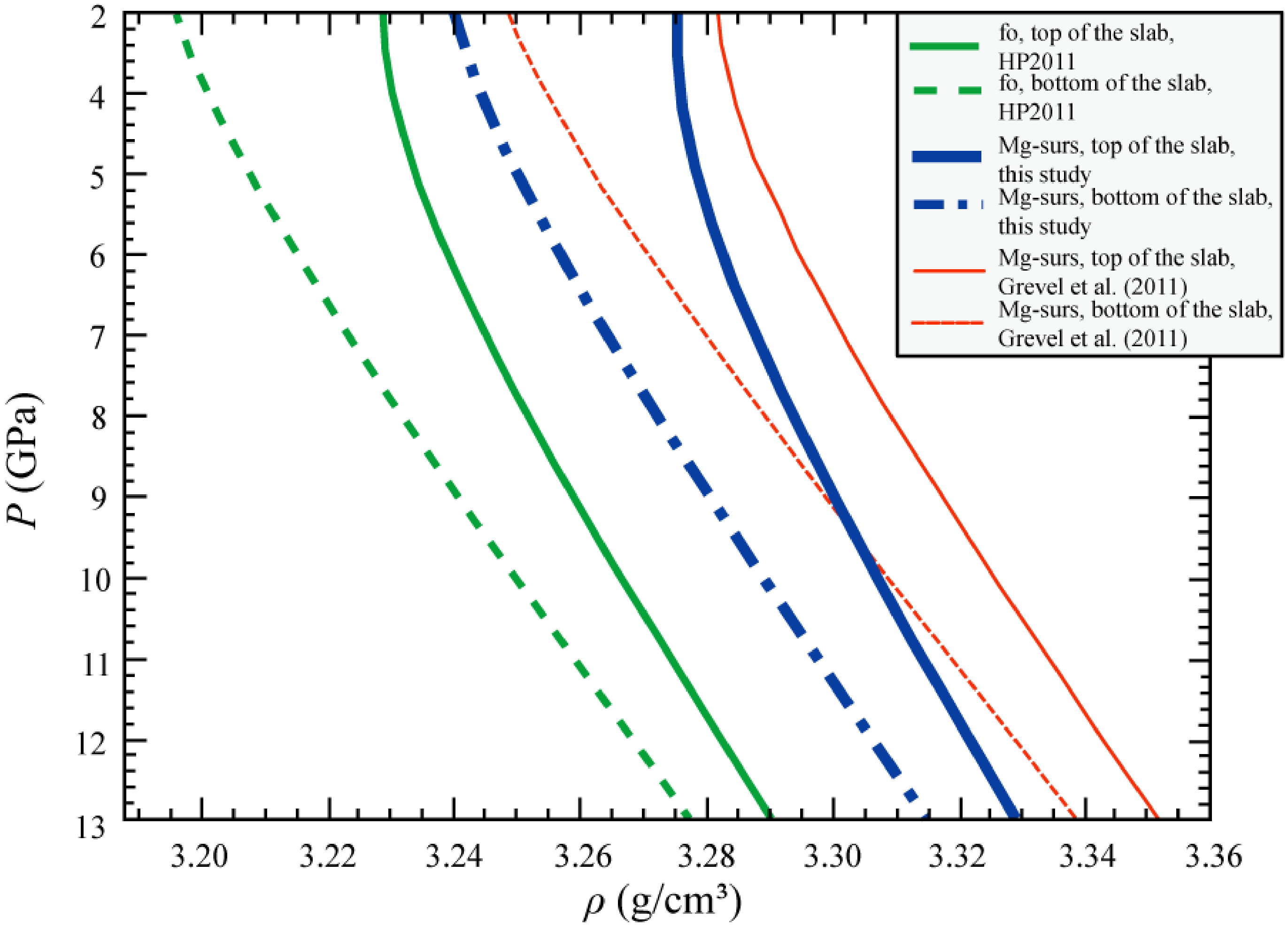
fo, top of the slab, HP2011
fo, bottom of the slab, HP2011
Mg-surs, top of the slab, this study
Mg-surs, bottom of the slab, this study
Mg-surs, top of the slab, Grevel et al. (2011)
Mg-surs, bottom of the slab, Grevel et al. (2011)
P (GPa)
2
4
5
6
7
8
9
10
11
12
13
3.20
3.22
3.24
3.26
3.28
3.30
3.32
3.34
3.36
ρ (g/cm³)